PROCEEDINGS OF SPIE

SPIEDigitalLibrary.org/conference-proceedings-of-spie

Fully integrated, standalone zero field optically pumped magnetometer for biomagnetism

J. Osborne, J. Orton, O. Alem, V. Shah

J. Osborne, J. Orton, O. Alem, V. Shah, "Fully integrated, standalone zero field optically pumped magnetometer for biomagnetism," Proc. SPIE 10548, Steep Dispersion Engineering and Opto-Atomic Precision Metrology XI, 105481G (22 February 2018); doi: 10.1117/12.2299197

SPIE.

Event: SPIE OPTO, 2018, San Francisco, California, United States

Fully Integrated, Standalone Zero Field Optically Pumped Magnetometer for Biomagnetism

J. Osborne, J. Orton, O. Alem[1], V. Shah[2]
QuSpin, Inc., Louisville, CO, USA 80027

ABSTRACT

We describe the operation and results of our first generation zero field optically pumped magnetometer (OPM) developed for biomedical applications. The OPM technology is one of the most promising non-cryogenic candidates to replace superconducting quantum interference device (SQUID) magnetometers in key areas of biomagnetism. The first-generation sensors are designed to transition OPM technology from a physics laboratory to researchers in the medical community. The laser and optical components are tightly integrated inside the sensor package, and the sensor is tethered to a dedicated electronics signal processing unit that enables automated and standalone operation inside a magnetically shielded room.

Keywords: Optically Pumped Magnetometer, Atomic Magnetometer, SQUID, Biomagnetism, Magnetoencephalography, and Magnetocardiography.

1. INTRODUCTION

The high sensitivity of superconducting quantum interference device (SQUID) magnetometers has enabled the field of Biomagnetism since its inception in the 1970s [1]. However, practical and cost constraints originating from cryogenic nature of the SQUIDs has impeded widescale adoption of the biomagnetic technologies.

A zero-field OPM with nearly 10 fT/√Hz level sensitivity was demonstrated as far back as in 1969 [2]. The subsequent discovery of alkali spin-exchange relaxation suppression in near-zero magnetic field environment provided the fundamental breakthrough necessary for miniaturization of zero field OPM technology [3]. Landmark work by Romalis and coworkers demonstrated OPM with sub-femtotesla level sensitivity using spin-exchange suppression in low magnetic fields [4]. More recently, development of integrated sensor packages [2], [5], [6] and head-to-head comparison between zero field OPMs and SQUIDs in a clinical setting have highlighted OPMs as a truly viable alternative to cryogenic technologies in many important clinical applications [5]–[9].

Here we describe the development of a fully integrated and automated zero field optically pumped magnetometer (QZFM) that can be used by the medical research community and other non-specialists in this field.

2. OVERVIEW

The basic architecture of QZFM is the same as that outlined in the Ref. [2], [10], [11] , and it utilizes zero-field level crossing resonance (Hanle) for operation. Figure 1 shows a schematic representation of sensor head.

A 795 nm, single mode vertical cavity surface emitting laser (VCSEL) resonant with the D1 line of ^{87}Rb is used for optical pumping and resonance detection. The optical output power of the laser is roughly 200 µW. The VCSEL is mounted on an electrically heated baseplate, and the temperature of the laser is stabilized at a mK level. The laser temperature and the laser injection current are controlled to precisely adjust the optical power and wavelength of the laser using digital feedback loops. The laser light is circularly polarized with a quartz waveplate, and the beam is collimated with a plano-convex lens. The collimated light beam is reflected 90 degrees using a prism and is then passed through a 3x3x3 mm^3 alkali vapor cell containing ^{87}Rb and a mixture of buffer gases to reduce rubidium relaxation from wall collisions. The light transmitted through the vapor cell is then directed by another prism towards a photodetector to

[1] presently at University of Colorado
[2] vshah@quspin.com www.quspin.com

Steep Dispersion Engineering and Opto-Atomic Precision Metrology XI, edited by Selim M. Shahriar, Jacob Scheuer, Proc. of SPIE Vol. 10548, 105481G · © 2018 SPIE · CCC code: 0277-786X/18/$18 · doi: 10.1117/12.2299197

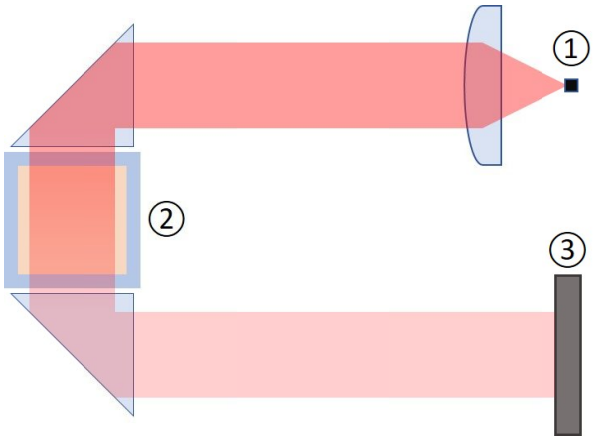

Figure 1: A laser diode **1** produces light that is tuned to the resonance frequency of the alkali atoms. The light beam is collimated and directed to pass through a glass cell **2** containing the vapor of alkali atoms. The transmitted light beam is directed onto a photodiode **3**.

monitor the light intensity transmitted through the vapor cell.

The vapor cell is electrically heated with resistive heaters to around 150 °C to optimize rubidium density. The vapor cell is ovenized to minimize heat loss and reduce the surface temperature of the outer sensor housing. The temperature of the vapor cell is actively stabilized at 10 mK level. All the components inside the sensor housing are chosen to be non-magnetic to the greatest extent possible. AC electrical currents are used to heat the laser and the vapor cell.

When the background magnetic field is zero, the circularly polarized laser light spin polarizes the rubidium atoms in the direction of the light beam propagating through the vapor cell, making rubidium atoms largely transparent to the incoming light. A magnetic field in a direction perpendicular to the light reorients the spins increasing the light absorption. The photodetector senses this change in transparency as a function of magnetic field and produces an electric current proportional to the light transmitted through the vapor cell. In this way, a magnetic signal is converted to an electric signal forming a zero-field magnetometer.

In zero field, if a magnetic field is applied in a direction perpendicular to the light beam and the amplitude of the transverse applied field is swept from a positive to a negative value, the transparency of the rubidium atoms changes such that maximum transparency is observed when the atoms experience a magnetic field that is very close to zero. The output of the photodetector as a function of the applied field has a Lorentzian line shape. This Lorentzian output is referred to as the zero-field or Hanle resonance (see Figure 2). In QZFM, the typical width (full width at half maximum

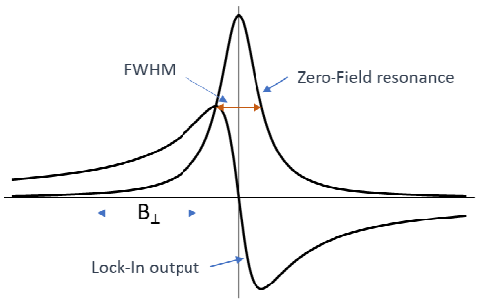

Figure 2: The zero-field resonance is the output of the photodetector as the magnetic field is scanned from a positive to a negative value in the direction perpendicular to the light beam through the vapor cell. The FWHM of the zero-field resonance in QZFM is around 30 nT. The demodulated output of the lock-in amplifier (also referred to as the error signal) has an asymmetric Lorenztian line shape.

– FWHM) of the zero-field resonance is around 30 nT.

To remove technical 1/f noise and to maximize the slope of the signal around zero field value, phase-sensitive lock-in detection is utilized. The atoms in the vapor cell are subjected to an oscillating magnetic field at 923 Hz which modulates the resonance. The modulated signal is synchronously demodulated using a lock-in amplifier producing an output that has an anti-symmetric Lorentzian line shape as seen in Fig. 2. The output of the lock-in amplifier has a maximum slope at zero field and functions as the raw analog output of the magnetometer.

The sensitive axis of the magnetometer is defined by the direction of the modulation field (projected on a plane perpendicular to the light beam). To make the magnetometer simultaneously sensitive to two orthogonal axes (perpendicular to the light beam), we apply two separate modulation fields (same frequency, 90 deg. phase offset) using separate orthogonal coils. Applying simultaneous modulation fields reduces the sensitivity in both axes by roughly 30%.

The residual magnetic field in a typical magnetically shielded room (MSR) is around 50 nT or lower. Because zero field OPMs require absolute zero field environment to operate, external field coils are necessary to cancel out any residual magnetic fields. To simplify the setup of QZFMs, we integrate field cancellation coils with the sensor package. A set of flexible three axis coils centered around the vapor cell is mounted over the sensor housing, and automated field-zeroing algorithms are used to cancel out any residual fields around the vapor cell. The field zeroing procedure is repeated whenever the direction or the magnitude of magnetic field changes by more than 1 nT or when the magnetometer orientation changes.

In QZFM, the internal coils are designed to compensate residual magnetic fields up to 50 nT. The primary limitation on the magnitude of the residual that can be canceled using internal coils comes from the stability and the noise performance of the internal coil drivers, as well as the inhomogeneity of the internal coils. The width of the zero-field resonance in QZFM is 30 nT. Therefore, transverse magnetic field gradients greater than ~10 nT over the length dimension of the vapor cell (3 mm) can substantially broaden the resonance width and degrade magnetometer performance.

3. MULTICHANNEL OPERATION AND CROSS-TALK

The QZFM is designed for multi-channel systems with high channel counts. Because the magnetic modulation signal used for lock-in detection can be picked up by adjacent sensors, we modulate all the sensors with a common drive signal to minimize interference. An electronics module designated as the ‘Master’ generates the modulation signal and distributes it to all other electronics modules designated as the ‘Slaves.’ Although deriving the modulation signals from a common drive resolves aliasing type effects, crosstalk effects are not fully removed by this procedure. Because the sensitive axis is defined by the direction of the modulation field, the modulation fields from adjacent sensors can superimpose on a sensor’s primary modulation field and thereby change the direction of the sensitive axis. Results from our preliminary experiments suggest such effects are at a few percent level when adjacent sensors are separated by >2-cm. The sensitivity of the magnetometer also depends on the amplitude of the modulation field. Superimposition of modulation fields from adjacent sensors also can also change the net amplitude/phase of modulation field experienced by a sensor, thereby changing the absolute sensitivity/accuracy of the sensor. Lastly, another cross-talk type effect that arises comes from the DC compensation coils on the sensor used for field zeroing. The internal three-axis field compensation coils used for field zeroing can produce a DC bias field that can be sensed by an adjacent sensor. Thus, running independent internal field zeroing algorithm in one sensor can push an adjacent sensor outside its operating field range. To alleviate this problem, we simultaneously run field zeroing procedure on all the sensors. Simultaneous field-zeroing collapses the overall system level DC field configuration in a way that each sensor experiences a zero-field environment to the greatest extent possible. The downside of this approach is that even if the position of a single sensor is reconfigured, the automated field zeroing procedure may have to be repeated for all the sensors.

4. ELECTRONICS CONTROLLER

The electronics control unit houses all the circuitry for controlling a QZFM sensor. A schematic overview of the QZFM electronics controller is shown in Figure 3. A VCSEL driver produces the low noise current to power the laser. A

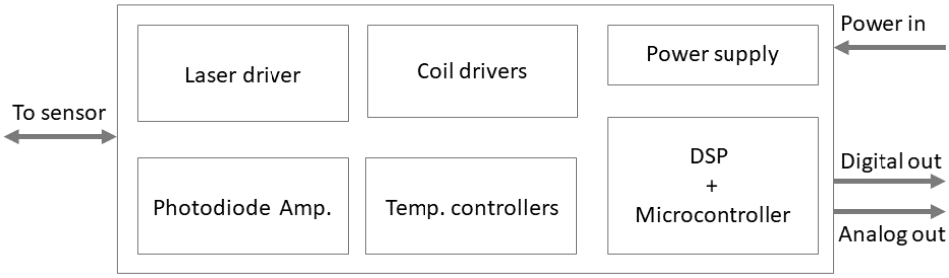

Figure 3: A schematic overview of the QZFM electronics controller. The electronics controller includes all the necessary components for stand-alone operation of a single QZFM sensor.

transimpedance amplifier is used to convert the photodiode current to voltage. The signal from the photodiode is digitized and read by a digital signal processor (DSP) that stabilizes the vapor cell and the laser temperature and generates lock-in outputs. The DSP also controls three low noise coil drivers to power the DC biasing coils for field zeroing. A microcontroller is used to boot the DSP, run algorithms for automated operation of the magnetometer, and to communicate with a host PC over a UART to USB bridge.

Figure 4 below shows a picture of the QZFM sensor head along with its electronics controller. The 6.5-meter cable

Figure 4: A picture of the QZFM sensor package and the control electronics.

connecting the sensor and the electronics housing allows the electronics to be placed outside the MSR.

5. RESULTS

The typical magnetic field sensitivity of QZFM is 10 fT/√Hz in 1-100 Hz frequency band as shown in Figure 5. The sensitivity in dual axis mode is roughly 30% lower compared with the sensitivity in single axis mode. Majority of the sensor units that we have built to date fall in a range between 7-13 fT/√Hz range in single axis mode. The typical -3 dB bandwidth of the sensor is 135 Hz, with a response roll-off similar to a first-order low-pass filter. In zero field, the sensor response is linear to within 1% when the signal amplitude is less than 1 nT.

In QZFM, the stand-off distance (see Figure 6) between the outside of the sensor housing and the center of the vapor cell is minimized to 6 mm. The small stand-off distance allows the sensors to be placed closer to a signal source compared with SQUID-based systems where the typical stand-off distance is 20-30 mm.

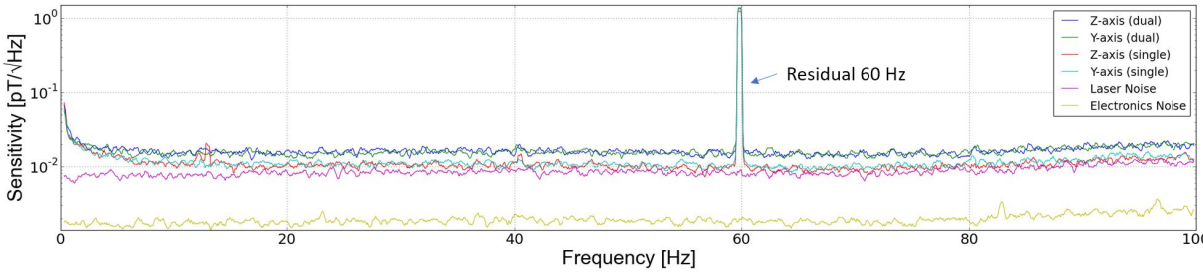

Figure 5: A typical noise floor of a QZFM measured inside a small 3-layer mu-metal magnetic shields with an inner ferrite layer. The noise traces include both single and simultaneous dual axis measurements.

The outside dimension of the sensor is 13x19x110 mm, and the electronics housing is 30x110x170 mm. The electronics unit is separated from the sensor head by a 6.5m cord allowing the electronics unit to be placed outside a magnetically shielded room if necessary. The electronics unit can also be placed a few feet away from the sensor inside the MSR without any noticeable interference. The total QZFM power consumption (including electronics) is 4.5 W, out of which ~700 mW is used to heat the vapor cell and the laser. The surface temperature on the subject facing surface of the sensor can rise by roughly 10 degrees C above ambient. The outside surface temperature partly depends on the thermal characteristics of the sensor holder.

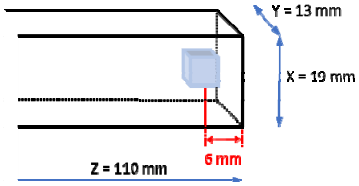

Figure 6: Position of the vapor cell with respect to the QZFM outer housing.

Unlike SQUID systems, there are no consumables (for example, liquid He) inside QZFM. Instead, the intrinsic lifetime is limited by the lifetime rating of the laser. The laser used in QZFM is rated for several years of continuous operation, although further long-term testing is needed in the context of QZFM which is highly sensitive to spectral and noise characteristics of the laser. In

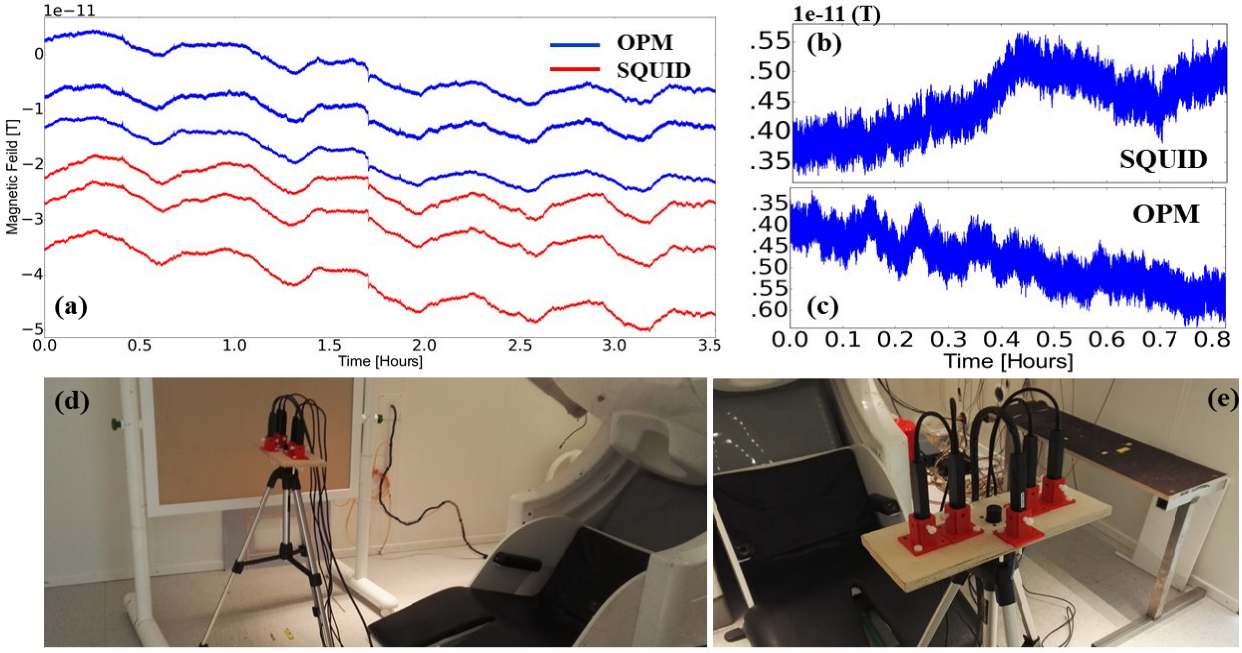

Figure 7: Low frequency performance of the QZFM. (a) Output of three free-running QZFMs and three (Elekta) SQUID magnetometers inside a three-layer shielded room. (b, c) Synthetic gradient between two adjacent SQUID magnetometers and QZFMs. (c) A picture showing placement of the Elekta MEG SQUID system and the QZFMs inside a MSR. The QZFMs shown in the background are roughly oriented to point in the same direction as SQUID magnetometers. (d) A close up photo of the QZFMs used in the measurements reported here.

addition, the QZFM is not hermetically sealed at present, and degradation of the surface quality of internal optics may place further constraints on the sensor lifetime.

Figure 7 shows the low-frequency performance of QZFM (data courtesy Joonas Iivanainen and Rasmus Zetter, Aalto University). The data was collected by recording the output of free running QZFMs inside a three-layer MSR. From the Figure 7(c), an upper bound on the intrinsic drift of QZFM is ~2 pT/hr. Figure 7 (b) and (c) show comparable drift in SQUID and OPM channels, potentially indicating that the measured drift may be due to changes in the gradient field.

A number of research groups have collected data MCG and MEG data using QZFM validating the technology in a clinical setting [5], [12], [13]. Figure 8 shows MEG recordings collected at the University of Wisconsin Madison (courtesy Prof. R. T. Wakai, University of Wisconsin) using an early version of the QZFM prototypes. A somewhat lower absolute sensitivity of QZFMs (10 fT/√Hz) compared with SQUIDs (3-5 fT/√Hz) is compensated by the smaller stand-off distance and proximal placement of the OPMs to the subject, providing equivalent or higher signal-to-noise

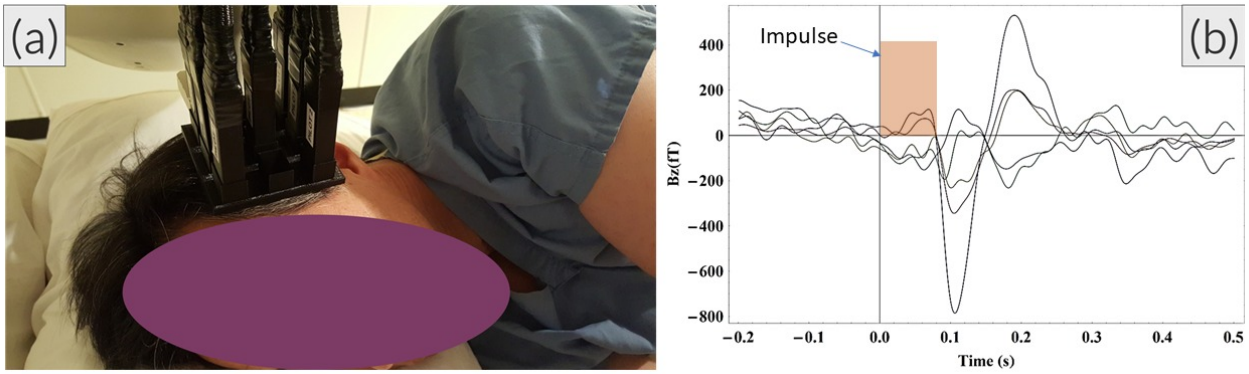

Figure 8: (a) A picture showing QZFMs positioned over the auditory cortex. (b) Auditory Evoked Response. Impulse spacing randomized 2-3 sec, 2 kHz tone, recording length 5 mins, ~175 averages.

ratios compared to SQUID systems.

6. CONCLUSION

We have demonstrated fully integrated, stand-alone zero field OPM sensors and shown that this technology is a truly viable alternative to SQUIDs sensors in key areas of biomagnetism such as fetal and adult MCG and MEG. The absolute sensitivity of our sensors is comparable to low-temperature SQUID devices. By integrating the laser diode and other optical components directly inside the sensor package, the overall robustness of the device is significantly improved allowing OPMs to be incorporated in routine clinical applications. In addition, integrating the laser diode with the sensor package has also greatly improved the sensor noise properties especially in the low-frequency domain. Furthermore, the addition of field zeroing coils inside the sensor has removed the need for external field zeroing infrastructure allowing the sensors to be used as stand-alone units inside a typical shielded room. We have also addressed many technical constraints enabling zero-field OPM operation in the multi-channel configuration for MEG type imaging applications. The non-cryogenic nature of OPM technology, combined with a highly simplified design is expected to provide a step change in technology for future biomagnetism applications.

7. REFERENCES

[1] D. Cohen, E. A. Edelsack, and J. E. Zimmerman, “MAGNETOCARDIOGRAMS TAKEN INSIDE A SHIELDED ROOM WITH A SUPERCONDUCTING POINT #x2010;CONTACT MAGNETOMETER,” *Appl. Phys. Lett.*, vol. 16, no. 7, pp. 278–280, Apr. 1970.

[2] J. Dupont-Roc, S. Haroche, and C. Cohen-Tannoudji, “Detection of very weak magnetic fields (10−9gauss) by 87Rb zero-field level crossing resonances,” *Phys. Lett. A*, vol. 28, no. 9, pp. 638–639, Feb. 1969.
[3] W. Happer and H. Tang, “Spin-Exchange Shift and Narrowing of Magnetic Resonance Lines in Optically Pumped Alkali Vapors,” *Phys. Rev. Lett.*, vol. 31, no. 5, p. 273, Jul. 1973.
[4] I. K. Kominis, T. W. Kornack, J. C. Allred, and M. V. Romalis, “A subfemtotesla multichannel atomic magnetometer,” *Nature*, vol. 422, no. 6932, pp. 596–599, Apr. 2003.
[5] V. K. Shah and R. T. Wakai, “A compact, high performance atomic magnetometer for biomedical applications,” *Phys. Med. Biol.*, vol. 58, no. 22, p. 8153, Nov. 2013.
[6] S. Knappe, T. H. Sander, O. Kosch, F. Wiekhorst, J. Kitching, and L. Trahms, “Cross-validation of microfabricated atomic magnetometers with superconducting quantum interference devices for biomagnetic applications,” *Appl. Phys. Lett.*, vol. 97, no. 13, p. 133703, 2010.
[7] O. Alem, A. M. Benison, D. S. Barth, J. Kitching, and S. Knappe, “Magnetoencephalography of Epilepsy with a Microfabricated Atomic Magnetrode,” *J. Neurosci.*, vol. 34, no. 43, pp. 14324–14327, Oct. 2014.
[8] C. Johnson, P. D. D. Schwindt, and M. Weisend, “Magnetoencephalography with a two-color pump-probe, fiber-coupled atomic magnetometer,” *Appl. Phys. Lett.*, vol. 97, no. 24, p. 243703, 2010.
[9] J. Sheng *et al.*, “Magnetoencephalography with a Cs-based high-sensitivity compact atomic magnetometer,” *Rev. Sci. Instrum.*, vol. 88, no. 9, p. 094304, Sep. 2017.
[10] R. E. Slocum and F. N. Reilly, “Low Field Helium Magnetometer for Space Applications,” *IEEE Trans. Nucl. Sci.*, vol. 10, no. 1, pp. 165–171, 1963.
[11] V. Shah, S. Knappe, P. D. D. Schwindt, and J. Kitching, “Subpicotesla atomic magnetometry with a microfabricated vapour cell,” *Nat Photon*, vol. 1, no. 11, pp. 649–652, Nov. 2007.
[12] E. Boto *et al.*, “A new generation of magnetoencephalography: Room temperature measurements using optically-pumped magnetometers,” *NeuroImage*, vol. 149, no. Supplement C, pp. 404–414, Apr. 2017.
[13] H. Eswaran, D. Escalona-Vargas, E. H. Bolin, J. D. Wilson, and C. L. Lowery, “Fetal magnetocardiography using optically pumped magnetometers: a more adaptable and less expensive alternative?,” *Prenat. Diagn.*, vol. 37, no. 2, pp. 193–196, Feb. 2017.